Numerical Analysis of an Insect Wing in Gliding Flight: Effect of Corrugation on Suction Side

Mohd Imran Ansari[1, *] and Syed Fahad Anwer[1]

Abstract: We have conducted a numerical study to investigate the relationship between the aerodynamic performance of an insect wing section and the effect of corrugation in gliding flight. In particular, an Airfoil-CR, corresponding to Kesel's Profile 2 (Kesel, Journal of Experimental Biology, vol. 203, 2000), has been used. This profile represents exactly the cross section of the so-called "Aeshna cyanea". A smoothed variant of this profile (referred to in the present study as Airfoil-SM) has also been considered. Introducing five different variants of the Airfoil-CR corresponding to different levels of corrugation, namely M1, M2, M3, M4 and M5, an unsteady fluid flow analysis has been carried out in the framework of a Fraction-Step Method (based on a velocity-pressure coupling scheme). Another airfoil M6 has also been considered by taking all the corrugations on the suction side simultaneously while the pressure side remains smooth. Simulations were performed for variety of Reynolds numbers ranging from 150 to 10000, while angle of attack was varied from 0° to 20°. According to the results, the performances (in terms of shear and pressure drags) change as a function of the corrugation and Reynolds number. While the performances of the Airfoil-CR are relatively good at low Reynolds numbers, its behavior changes completely at higher Reynolds number where the best performances are achieved by using the Airfoil-SM. Moreover, steady or oscillatory flow can emerge depending on the considered situations.

1 Introduction

Micro-Air-Vehicle (MAV) is an important research topic in current century due to its wide range of application like intelligence, surveillance, reconnaissance and in hazardous environments. MAV belongs to the miniature class of unmanned air vehicles. The idea of research in design of MAVs is inspired from the flight of insects. The research on MAVs helps to understand the nature of insect flights and aid in development for practical uses such as flying through cracks in concrete, search for earthquake victims or exploring radioactive-contaminated buildings. Spy agencies and military also appreciate potential for such small vehicles as spies and scouts. Typical MAVs can have size as small as 15 cm, weighs about 90 g and have flight speeds usually ranging between 2 m/s to 10 m/s.

---

[1] Zakir Husain College of Engineering & Technology, Aligarh Muslim University, Aligarh, 202002, India.

[*] Corresponding Author: Mohd Imran Ansari. Email: mailimran99@gmail.com.

Most of the studies for design of micro air vehicles are performed by analyzing the flying manoeuvrability of insect such as Fruit-fly, Del-fly, Dragonfly and Bumble bee etc. Among different insects, the aspect ratio of wing is highest for dragonfly [Ellington (1984b); Vogel (1957)].

Among insects, dragonflies are functionally and morphologically different having two pairs of wings which results in good manoeuvrability. Due to high aspect ratio of the wing, dragonfly is an important research topic for design of MAVs. Dragonfly uses powered (flapping) flight to elevate in the air and uses potential energy to move horizontally above the ground [Brodsky (1994)]. The flapping frequency are in the range of 30 Hz to 50 Hz [Ruppell (1989)] and motion of forewing and hindwing are independent [Alexander (1984)]. The typical Reynolds number for dragonfly lies between 100 and 10000 [Wakeling and Ellington (1997a)]. The flow at these low Reynolds numbers have large unsteady vortical flow structures and have both inertia and viscous forces effective. Reynolds number highly influences the structure and stability of these vortices which creates low pressure region, due to which the aerodynamic lift force is enhanced [Birch and Dickinson (2001); Shyy and Liu (2007)]. For MAVs, the gliding flight is more efficient as it require no energy consumption [Vargas and Mittal (2004)]. The efficient gliding performance of a dragonfly wing is due to its high aspect ratio. The wings of dragonfly are not smooth or simple cambered surfaces but have some corrugated configuration which varies along chord and span of the wing [Kesel (1998); May (1991); Mingallon and Ramaswamy (2011); Okamoto, Yasuda and Azuma (1996); Vargas, Mittal and Dong (2008); Wootton (1992)]. Corrugated wing provides the structural advantage of high stiffness while allowing torsion to occur and also have low mass [Ennos (1995); Kesel, Philippi and Nachtigall (1998); Norberg (1972)]. A significant experimental study was performed by Kesel [Kesel (2000)] on dragonfly (*Aeshna cyanea*) and it was reported that corrugated wing have very low drag coefficient and a greater lift coefficient as compared to a flat plate. A negative pressure was produced on both sides in the profile valleys and therefore the net negative pressure on upper side was obtained at angle of attack greater than 0°. Numerical simulations on a wing of a dragonfly under gliding mode at low Reynolds number was performed by Vargas et al. [Vargas, Mittal and Dong (2008)]. They found that the negative shear drag produced by the recirculation zone within the pleats reduces the overall drag. And pleated airfoils have higher lift and moderate drag results compared to profiled airfoil. Finally they concluded that the pleated wing is an ingenious design of nature. Kim et al. [Kim, Ko, Park et al. (2009)] analyzed 2D corrugated wing and found that the lift coefficient increases (except at angle of attack $\alpha=0°$); and a little influence on drag coefficient of corrugated wing at all Reynolds number was perceived. The vortex in valley and near the edge of corrugation were locally different from those of an elliptic wing. Meng et al. [Meng and Sun (2013)] studied different corrugated profiles and compared them with flat plate in gliding motion. They found the negative effect of corrugation on aerodynamic performance with slight change in drag and considerable decrease in lift. The possible reasons cited for reduction in lift are relatively strong vortices on lower surface of corrugated wing due to pleats, and the corrugation near the leading edge pushing the leading-edge-separation layer slightly upwards and increasing the size of the separation bubble above the upper surface. Tuncer et al. [Tuncer and Kaya (2003)] studied the

laminar and turbulent flow over the flapping airfoils in a biplane configuration undergoing pure plunge and combined pitch and plunge motion. They found that in the flapping airfoils 20-40% more thrust is produced in a biplane configuration with a proper phase shift in a combined pitch and plunge motion, than single flapping airfoil. Chen et al. [Chen and Skote (2016)] carried out CFD analysis of 3D corrugated wing while considering the variation of corrugation along spanwise direction. They compared the effect of corrugation with smoothly profiled counterpart in gliding flight with primary focus on the effect of three-dimensionality as compared to 2D modeled wing. They found that variation of leading edge orientation along spanwise direction prevents the non-realistic oscillations on lift and drag. Strong spanwise flow stabilized the vortex formed on the leading edge and prevents its shedding into wake.

In a 2D model, only the cross-sectional plane is considered, while the thickness of model wing and orientation of leading edge along the spanwise direction are neglected, which are otherwise taken in account in a 3D model. Therefore the performance of wing due to effect of leading edge variation along the spanwise direction is not captured [Chen and Skote (2016)]. Present study is purely done for the comparison between the effects of different corrugations on the suction side of the airfoil. In this paper, a 2D section at 50% relative span length from the wing base of dragonfly *Aeshna cyanea* is selected (corresponding to Kesel's Profile 2 [Kesel (2000)]). Seven airfoil are then constructed from this basic profile. Numerical simulations of various airfoils is carried out for forward flight in gliding to find the effect of different corrugations on the suction side of the wings and subsequently analyze and compare the aerodynamic performance.

2 Numerical methods

2.1 Governing equations

The time dependent Navier-Stokes equation, governing the viscous incompressible flow, are used in the solver. The continuity and momentum equations are as follows:

Continuity:
$$\nabla . \vec{u} \quad = 0 \tag{1}$$
Momentum:
$$\frac{\partial \vec{u}}{\partial t} + \vec{u} . \nabla \vec{u} = -\nabla p + \frac{1}{Re} \nabla^2 \vec{u} \tag{2}$$
Where, Re is the Reynolds number based on chord length 'c', 'ρ' is the density of fluid, 'U_∞' is the free stream velocity and 'μ' is the dynamic viscosity. Reynolds number is defined as:
$$Re = \frac{\rho U_\infty c}{\mu} \tag{3}$$
The equation governing the flow is solved by Finite Volume Method (FVM). The staggered transient pressure based solver is used with Fractional Step Method (FSM) as the pressure-velocity coupling scheme with Non-Iterative Time Advancement (NITA). The FSM uses pressure based segregated algorithm. Using operator-splitting technique, momentum equations were decoupled from continuity equation. In NITA scheme the transient simulation speed up, as each set of equation is solved using inner iteration and only one outer iteration per time step. On a staggered grid the scalar variables (pressure, density, total enthalpy etc.) are stored in the cell centers of the control volumes, whereas

the velocity or momentum variables are located at the cell faces. The convective and diffusive terms are discretized using Quadratic Upstream of Convection Kinetics (QUICK) scheme, which is a second order central difference for diffusive term, third order accurate in space and first order in time for convective term. The code was modified from Anwer et al. [Anwer, Hasan and Sanghi (2009); Hasan, Anwer and Sanghi (2005)] to include finite volume and staggered grid methodology. The coding was done in Fortran 90 and runs were performed on i7 based machines.

2.2 Airfoil geometries

The corrugated biological airfoil extracted from the paper of Kesel [Kesel (2000)], where it corresponds to Profile 2 with cross-section at relative span length l_{rel}=0.5 (or 50%) from the base of the dragonfly (Aeshna cyanea) forewing as shown in Fig. 1(a). The suction and pressure sides, both have five corrugation each. Firstly, by taking the extreme corner points on the corrugated profile designated as CR, a smooth profile SM is constructed by fitting splines along these extreme corner points. Secondly, different profiles are constructed by considering the different corrugation separately each on the suction side of the corrugated profile, while remaining portion of suction side and pressure side of the profile remains smooth. Thirdly, Airfoil-M6 is constructed by taking the suction side fully corrugated and pressure side fully smooth. The different geometries of the profiles are shown in Fig. 1(b). The purpose of corrugation at different points according to section of Airfoil-CR is to compare the corrugation or pleat which is more effective to aerodynamic performance at various Reynolds number.
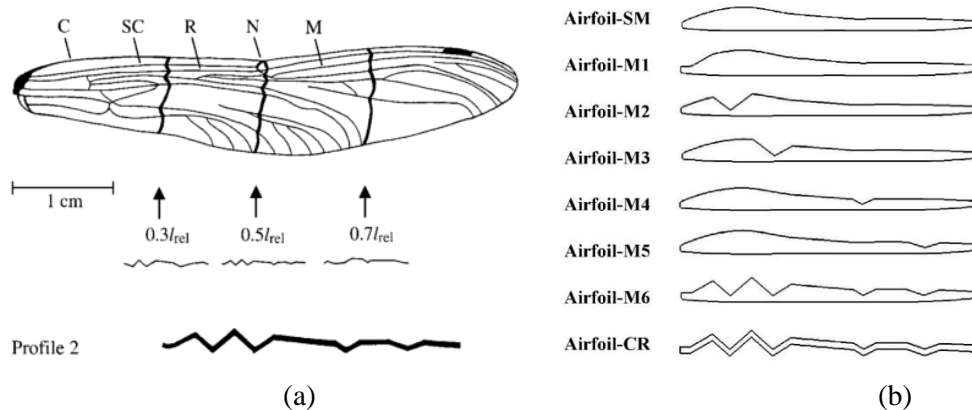

Figure 1: (a) Fore-wing of dragonfly *Aeshna cyanea* and Profile 2 at $0.5l_{rel}$ section of the wing [Kesel (2000)] **(b)** Different two-dimensional Airfoil geometries having t/c=7.531%

Airfoil-SM with smooth upper and lower curves is the simplest airfoil having no corrugation and Airfoil-CR is the most complicated among the considered profiles, representing the extreme reference profiles as shown in Fig. 1(b). Airfoil-M6 have the whole upper surface corrugated while whole of the lower surface is smooth. Airfoils M1 to M5 represents the corrugation on the upper surface separately and are compared for aerodynamic performance with airfoil CR and SM. All the airfoils have thickness to chord length ratio t/c=7.531%.

2.3 Boundary conditions

To solve the discretized governing equations, boundary conditions must be defined for the computational domain. The two-dimensional circular computational domain of diameter 60c is built with an airfoil at its center as shown in Fig. 2. A Dirichlet-type boundary condition is defined having fluid velocity inlet to the domain of 1m/s in x-direction and zero velocity in y-direction at left half-circle, while the right half-circle of zero gauge pressure is applied as the boundary condition. The wall with no-slip boundary condition is applied to the surface of the wing.
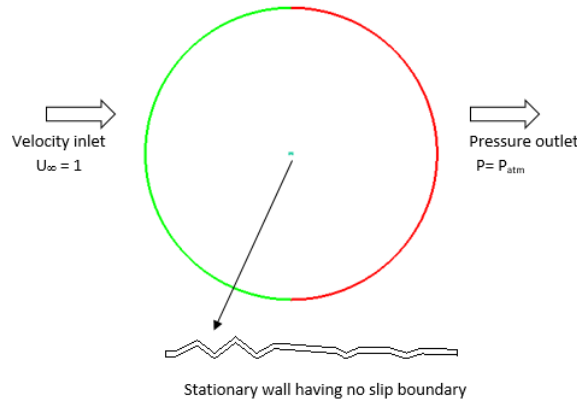
Figure 2: Computational domain with boundary condition

2.4 Computational grid

The computational circular domain is discretized by using O-type structured grid. The diameter of domain is 60c, which is finally selected after comparing with domain of diameter 40c, 60c and 80c having the value of force coefficient less than 0.5% between 60c and 80c. The grid has 70446 (354×199) Quadrilateral cells. The distance between the airfoil surface and the first layer of the grid is 0.0001c. Three computational grid of size 50622, 70446 and 105492 quadrilateral cells were formed to study the grid independence at 4° angle of attack for the most corrugated airfoil (CR) at Re=6000. Final grid for simulation should be selected such that the lift and drag forces change within 5% as shown in Tab. 1. The numerical simulation in all cases is performed at 70446 quadrilateral cell grid and uniform time step of $0.0005c/U_\infty$.

Table 1: Grid independence test for Airfoil-CR at 4° angle of attack and Re=6000

Airfoil-CR, Re=6000 and Angle of attack=4°						
S. No.	Quadrilateral cells	Grid size	$\bar{C}_L$	$\bar{C}_D$	% change in $\bar{C}_L$	% change in $\bar{C}_D$
1	50622	0.0005	0.3475	0.0693	-	-
2	70446	0.0001	0.3583	0.0709	3.097	2.483
3	105492	0.00005	0.3641	0.0727	1.619	2.474

2.5 Validation

In order to validate the current pressure based solver, the numerical simulation for the flow past NACA 0004 airfoil were performed and results are compared with Kunz et al. [Kunz and Kroo (2001)]. The result of interest is lift and drag coefficients. The time averaged lift and drag coefficients at 0° and 4° angle of attack and Re=2000 and 6000 are tabulated in Tab. 2.

Table 2: Numerical value of C_L and C_D for NACA0004 in comparison with Kunz et al. [Kunz and Kroo (2001)] for Re=2000 and 6000 at 0° and 4°

Angle of attack (degree)	α=0°				α=4°			
Reynolds Number	Re=2000		Re=6000		Re=2000		Re=6000	
	$\bar{C}_L$	$\bar{C}_D$	$\bar{C}_L$	$\bar{C}_D$	$\bar{C}_L$	$\bar{C}_D$	$\bar{C}_L$	$\bar{C}_D$
Numerical results	-	0.07102	-	0.03968	0.3191	0.076	0.3315	0.04403
Kunz & Kroo (2001)	-	0.0704	-	0.0392	0.335	0.0749	0.3439	0.0427
Percentage difference	-	0.88	-	1.22	4.74	1.18	3.6	3.11

From Tab. 2, it is clearly evident that the result for NACA 0004 airfoil obtained by present solver and that of Kunz et al. [Kunz and Kroo (2001)] have the difference in C_L and C_D less than 5% for all the four cases. This means that the current pressure based solver is suitable for numerical simulations.

3 Results and discussion

3.1 Force coefficients

Unsteady aerodynamic performance study has presently been carried out to investigate the effect of corrugation on 2D section on suction side of a dragonfly wing. The biological corrugated airfoil for dragonfly (*Aeshna cyanea*) forewing at $0.5l_{rel}$ is extracted from paper of Kesel [Kesel (2000)], where it corresponds to Profile 2. The study consists of considering each corrugation separately on suction side and comparison with smooth Airfoil-SM and corrugated Airfoil-CR. The force coefficient for 2D airfoils are calculated using the following relations.
Lift coefficient:
$$C_L = \frac{L}{\frac{1}{2}\rho U_\infty^2 c} \tag{4}$$
Drag coefficient:
$$C_D = \frac{D}{\frac{1}{2}\rho U_\infty^2 c} \tag{5}$$
Where, L and D corresponds to lift and drag forces generated on an airfoil of chord length c having incoming flow velocity U_∞.

The time averaged mean lift and drag coefficient is calculated by taking average of transient stationary part of $C_L(t)$ and $C_D(t)$.

Mean lift coefficient:

$$\bar{C}_L = \frac{1}{T-t_o} \int_{t_o}^{T} \frac{F_L(t)}{1/2\rho U_\infty^2 c} \, dt \tag{6}$$

Mean drag coefficient:

$$\bar{C}_D = \frac{1}{T-t_o} \int_{t_o}^{T} \frac{F_D(t)}{1/2\rho U_\infty^2 c} \, dt \tag{7}$$

Where 't_o' be time for simulation at which the transient stationary state is start and 'T' is time when 20 cycles of oscillations time is add up.

Total time averaged mean drag $\bar{C}_D$ for the airfoil is composed of drag due to pressure ($\bar{C}_{DP}$) and due to shear (mean skin friction coefficient) on the surface ($\bar{C}_{SF}$). By neglecting the induced drag for 2D geometry, the total time averaged mean drag coefficient is given by:

Total time averaged drag:

$$\bar{C}_D = \bar{C}_{DP} + \bar{C}_{SF} \tag{8}$$

Fig. 3 shows oscillation of lift and drag coefficient with angle of attack for corrugated airfoil at various Reynolds number.

(a)

(b)
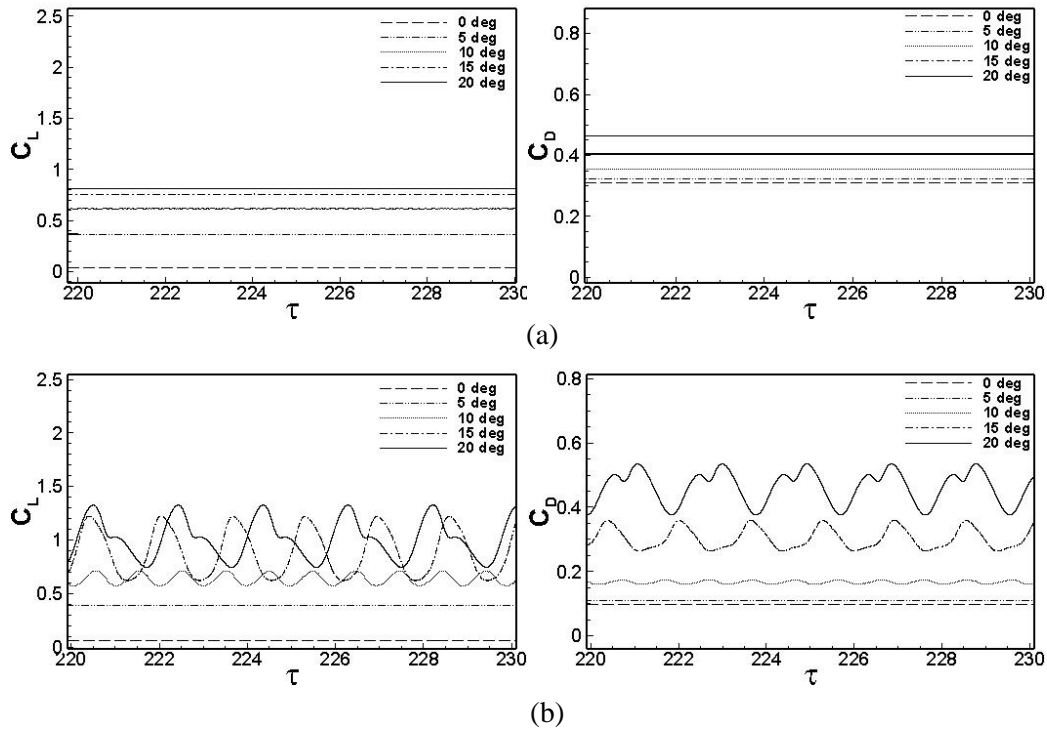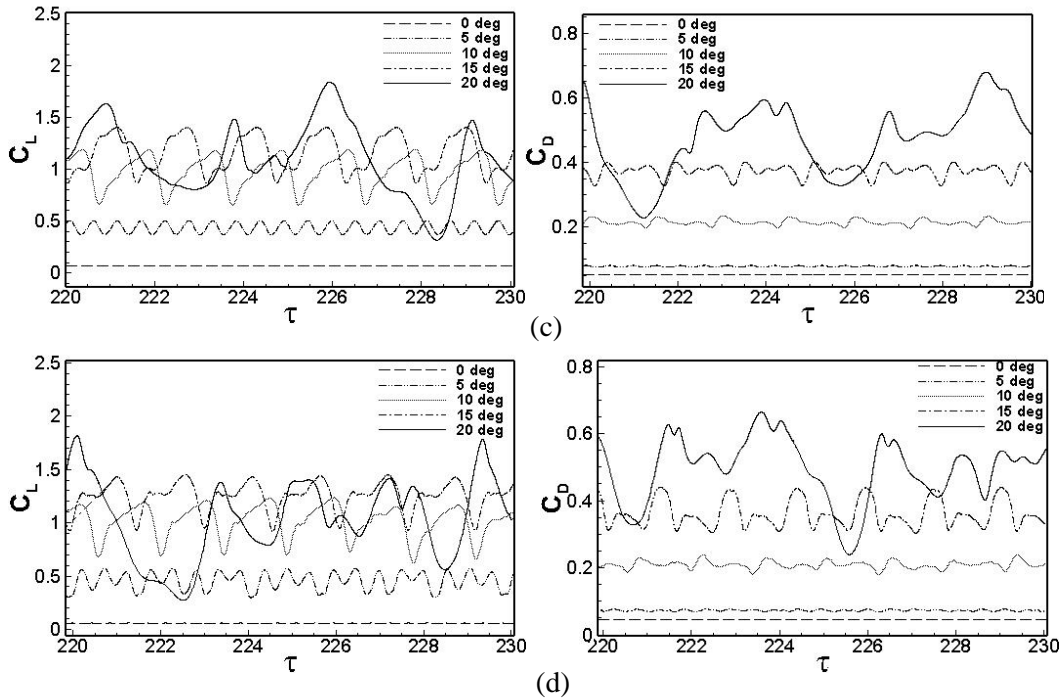
Figure 3: Variation of lift and drag coefficient for Airfoil-CR at (a) Re=150 (b) Re=1400 (c) Re=6000 and (d) Re=10000

The time histories of lift and drag coefficient of the flow are straight lines indicating that the flow around the airfoils is steady in nature at Re=150 for the range 0° to 20° angle of attack. At Re=1400, the flow is steady up to 5° angle of attack, and thereafter at higher angles of attack the flow becomes oscillatory in nature. The amplitude of oscillation increases and frequency of cycle decreases with advancement in the angle of attack. The oscillatory flow is due to change in the vorticity field formed on the upper surface of the wing and flow becomes unsteady. For Re=6000, the flow is steady at 0° having no oscillation but the flow become oscillatory at 5° and higher angles of attack. The flow is totally oscillatory even at 0° angle of attack for Re=10000 except airfoil SM and M4 for which time history of lift and drag coefficient are straight lines as shown in Fig. 4. This indicates that at 0° angle of attack and Re=10000, the corrugation on the wing surface is responsible for oscillatory nature and the flow becomes unsteady. The corrugation corresponding to airfoil M4 have similar behavior and lift and drag coefficient values are also nearly same. The Strouhal number (St =fc/U_∞, where f is frequency of oscillation) for the oscillating flow in case of airfoil CR becomes 2.24, 1.92, 0.70, 0.65 and 0.46 for angle of attack α=0°, 5°, 10°, 15°and 20° respectively.
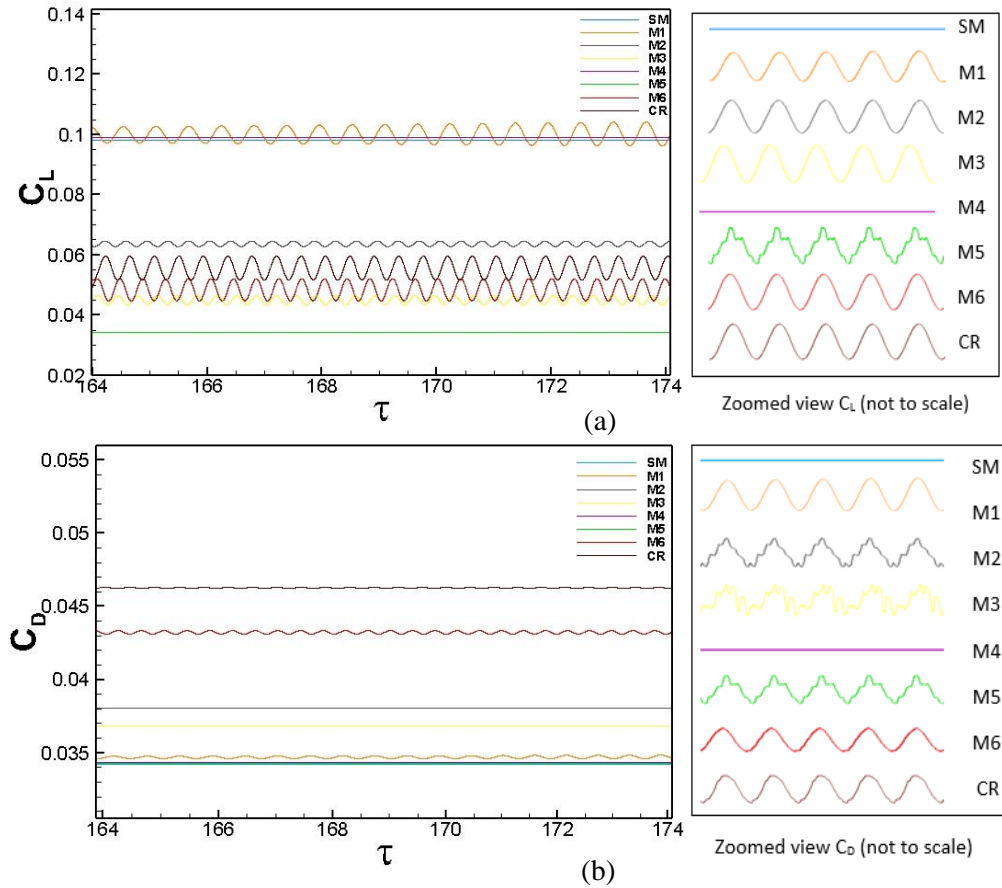
Figure 4: Variation of (a) lift and (b) drag coefficient for various airfoils at Re=10000

3.2 Effect of angle of attack

A range of 0° to 20° in steps of 5° increment is selected for the analysis of effect of angle of attack. The lowest lift and highest drag at Re=150 and highest lift and lowest drag is found at Re=10000. The time averaged mean force coefficient at 0° for airfoils at various Reynolds number are tabulated in Tab. 3.

Table 3: Time averaged mean force coefficient and gliding ratio at 0° angle of attack and Re=150, 1400, 6000 and 10000

Angle of attack=0° and Re=150						
Airfoil	$\bar{C}_L$	$\bar{C}_D$	$\bar{C}_{DP}$	$\bar{C}_{SF}$	$\bar{C}_L/\bar{C}_D$	% $\bar{C}_{SF}$
SM	0.0336	0.3147	0.0527	0.2619	0.1069	83.22
M1	0.029	0.3141	0.0566	0.2575	0.0925	81.98
M2	0.0274	0.313	0.0648	0.2483	0.0876	79.33
M3	0.0307	0.3137	0.0581	0.2556	0.0979	81.48

Airfoil	$\bar{C}_L$	$\bar{C}_D$	$\bar{C}_{DP}$	$\bar{C}_{SF}$	$\bar{C}_L/\bar{C}_D$	% $\bar{C}_{SF}$
M4	0.0331	0.3147	0.0542	0.2604	0.1053	82.75
M5	0.0486	0.3137	0.0537	0.2601	0.1545	82.91
M6	0.0136	0.3131	0.0926	0.2205	0.0436	70.42
CR	0.0405	0.3104	0.1405	0.1699	0.1306	54.74

Angle of attack=0° and Re=1400

Airfoil	$\bar{C}_L$	$\bar{C}_D$	$\bar{C}_{DP}$	$\bar{C}_{SF}$	$\bar{C}_L/\bar{C}_D$	% $\bar{C}_{SF}$
SM	0.0515	0.0935	0.0243	0.0692	0.5502	74.01
M1	0.0488	0.0935	0.0271	0.0664	0.5225	71.02
M2	0.044	0.0939	0.0314	0.0625	0.4682	66.56
M3	0.0481	0.094	0.0272	0.0668	0.5113	71.06
M4	0.0507	0.0936	0.0247	0.069	0.5417	73.72
M5	0.0589	0.0932	0.0246	0.0686	0.632	73.61
M6	0.0363	0.0959	0.046	0.0498	0.3785	51.93
CR	0.0619	0.0965	0.0702	0.0263	0.641	27.25

Angle of attack=0° and Re=6000

Airfoil	$\bar{C}_L$	$\bar{C}_D$	$\bar{C}_{DP}$	$\bar{C}_{SF}$	$\bar{C}_L/\bar{C}_D$	% $\bar{C}_{SF}$
SM	0.0712	0.0442	0.0168	0.0275	1.6094	62.22
M1	0.0756	0.0444	0.0197	0.0246	1.7049	55.41
M2	0.0555	0.0465	0.0228	0.0237	1.1923	50.97
M3	0.0518	0.0459	0.0181	0.0278	1.1283	60.57
M4	0.0722	0.0444	0.0168	0.0276	1.6287	62.16
M5	0.0719	0.0441	0.017	0.0271	1.6311	61.45
M6	0.0514	0.05	0.0342	0.0158	1.0273	31.60
CR	0.0661	0.0524	0.0511	0.0012	1.2623	2.29

Angle of attack=0° and Re=10000

Airfoil	$\bar{C}_L$	$\bar{C}_D$	$\bar{C}_{DP}$	$\bar{C}_{SF}$	$\bar{C}_L/\bar{C}_D$	% $\bar{C}_{SF}$
SM	0.0981	0.0342	0.0153	0.0189	2.865	55.26
M1	0.1023	0.0348	0.0186	0.0162	2.9366	46.55
M2	0.0637	0.0381	0.0217	0.0163	1.6743	42.78
M3	0.045	0.0368	0.0157	0.0211	1.2214	57.34
M4	0.0991	0.0343	0.0151	0.0192	2.8867	55.98
M5	0.1041	0.0343	0.0156	0.0187	3.037	54.52
M6	0.0484	0.0432	0.0328	0.0105	1.1203	24.31
CR	0.0557	0.0463	0.0474	-0.0011	1.2027	-2.38

The total time averaged mean drag coefficient increases with decrease in Reynolds number because at low Reynolds number viscous forces are dominant and therefore the skin forces adds up to the overall drag coefficient. The corrugated airfoil CR has trapped vortices in which flow is rotating in corrugated valleys causing reduction in shear drag.

The percentage of shear drag for various airfoils at different Reynolds number is also shown in Tab. 3. It is found that airfoils M6 and CR have low percentages of drag at all Reynolds number in which airfoil CR have the lowest. This means that corrugation on the surface of airfoil is responsible for the decrease in shear drag. The percentage of shear drag decreases with increase in Reynolds number. At Re=150, airfoils M6 and CR have the lowest values of 70.42% and 54.74%, while other airfoils have comparable values in the range of 79% to 83%. As the Reynolds number increases to 1400, there is also decrease in shear drag for airfoil M2 as compared to other airfoils, but higher than M6 and CR. Corrugation corresponding to airfoil M1 becomes effective at Re=6000, have smaller value of shear drag but larger than M2, M6 and CR. At Re=10000, shear drag becomes slightly negative for airfoil CR, which means that the direction of the shear drag reverses. Airfoils SM, M3, M4 and M5 have comparable shear drag values, and higher shear drag in comparison to airfoils M1, M2, M6 and CR. This means that the corrugation near leading edge becomes effective at higher Reynolds number. From the above results it is inferred that shear drag contribution decreases with increase in Reynolds number and Airfoil-SM has highest shear drag while Airfoil-CR have the lowest. Comparing the airfoils M1 to M6, the lowest shear drag is found in Airfoil-M6, and when comparing the airfoils having single corrugation, Airfoil-M2 has the lowest shear drag.

Fig. 5 shows the variation of lift coefficient with angle of attack at various Reynolds number.

The lift coefficient increases with an increase in angle of attack for Re=150 and 1400 while for Re=6000 and 10000 the lift coefficient drops in between 15° and 20° angle of attack. From the figure it is clearly observed that Airfoil-CR has highest lift coefficient among the airfoils at Re=150 and Re=1400. Airfoil-M6 with fully corrugated suction side has a lowest lift coefficient while the other airfoils have nearly same value of lift coefficient. The variation of lift coefficient with drag coefficient at various angle of attack and Reynolds number has been shown in Fig. 6. The lift coefficient increases with increase in drag coefficient initially and decline after 15° angle of attack for Re=6000 and 10000 similar to Fig. 5. It is to be noted here that on any curve on the graph the depicted values of $\bar{C}_L$ at a particular value of $\bar{C}_D$ represents five angles of attack in range 0° to 20° in steps of 5°. It is observed that each curve in the graph has higher slope initially and thereafter at higher angles the slope decreases and graph falls after 15° angle of attack for Re=6000 and 10000. This indicate that stalling of the airfoil occur after 15° angle of attack.
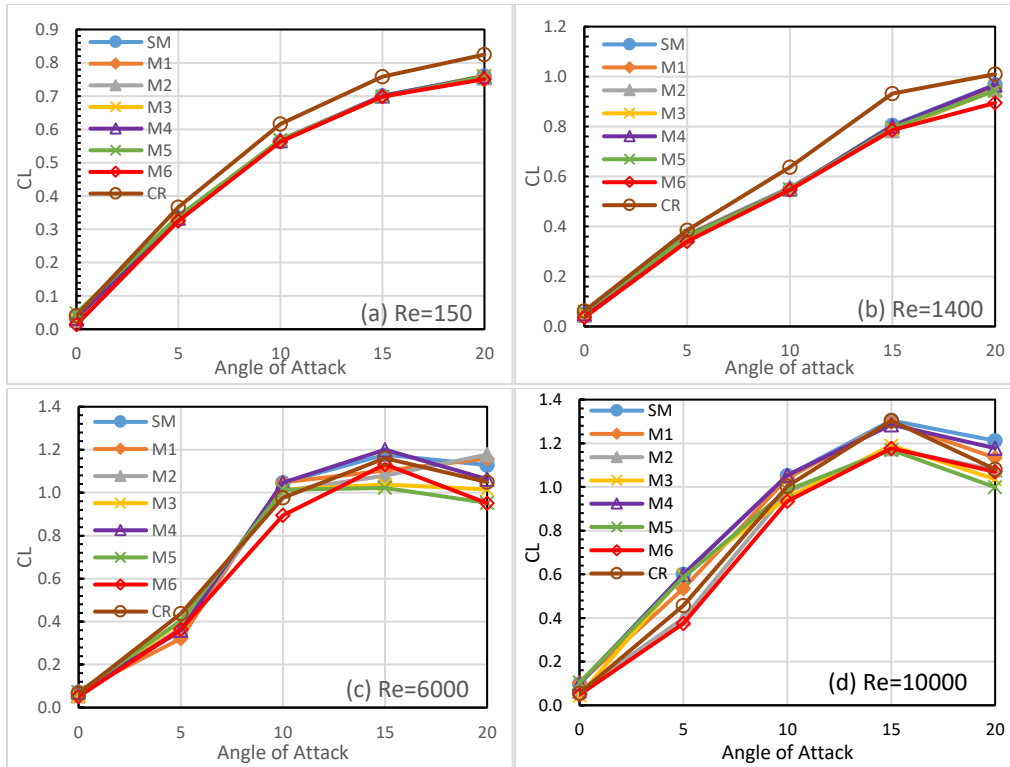
Figure 5: Variation of time averaged mean lift coefficient ($\bar{C}_L$) with angle of attack for various airfoils at (a) Re=150 (b) Re=1400 (c) Re=6000 & (d) Re=10000
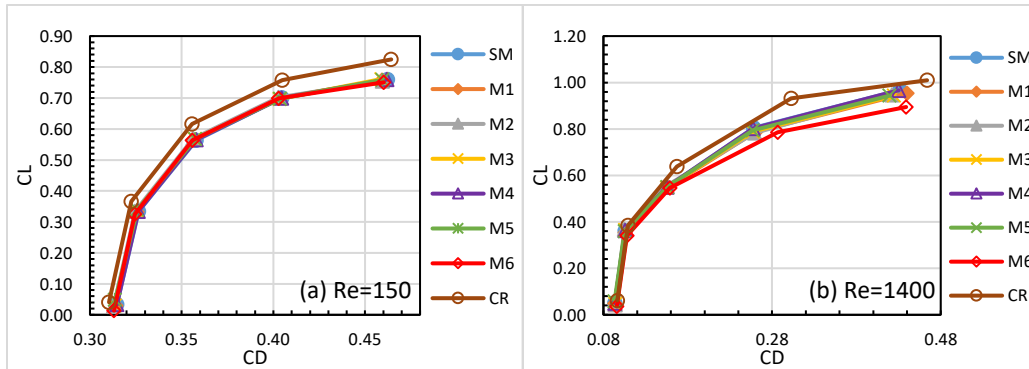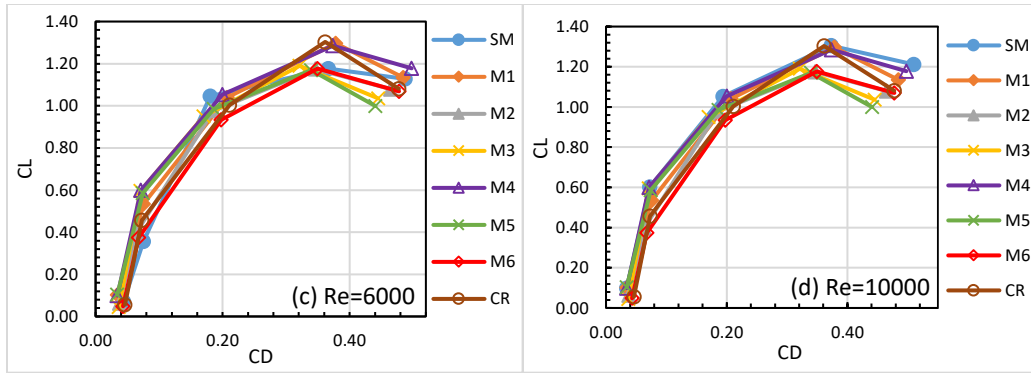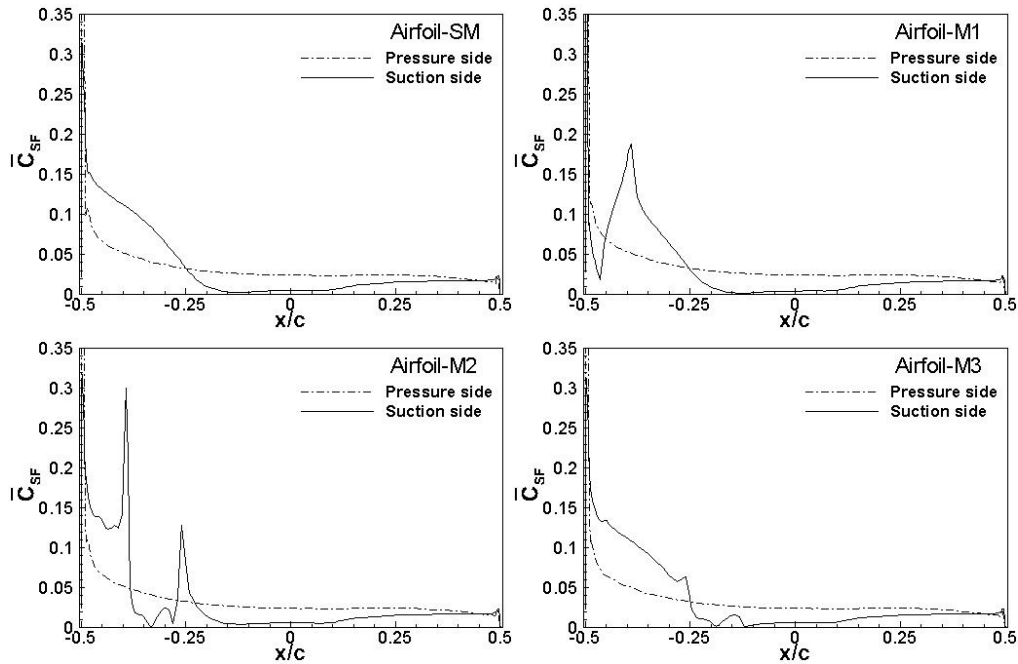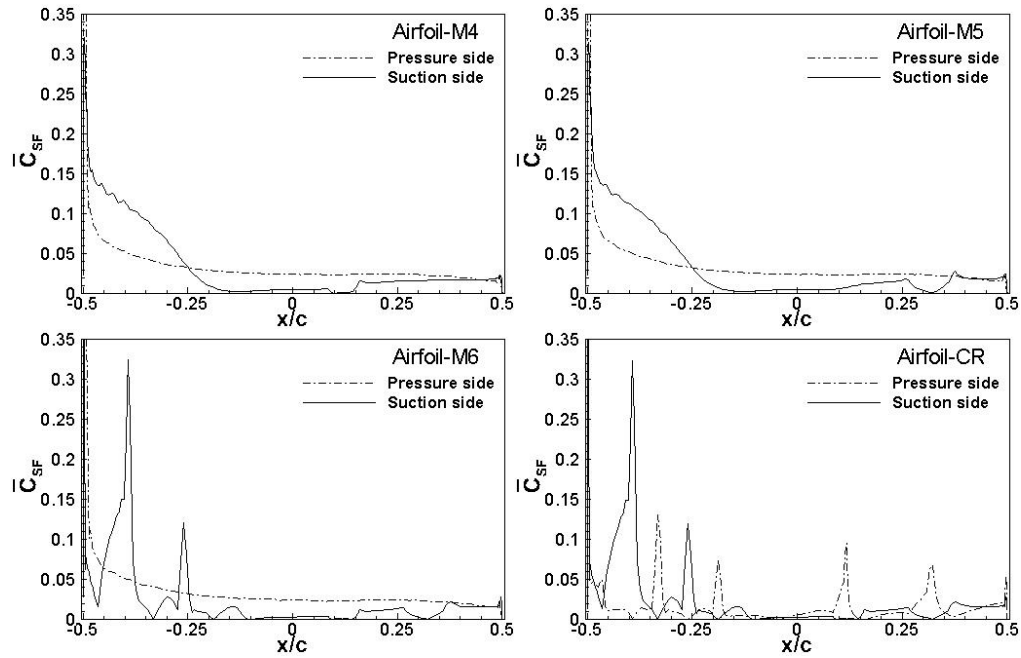
Figure 6: Variation of time averaged lift coefficient $\bar{C}_L$ with drag coefficient $\bar{C}_D$ for various airfoils at (a) Re=150 (b) Re=1400 (c) Re=6000 and (d) Re=10000

3.3 Effect of corrugation

It is of interest to study the effect of corrugation on the surface of airfoil. For this, airfoil M1, M2, M3, M4 and M5 are compared for corrugations at different positions on suction side corresponding to Airfoil-CR. Furthermore the Airfoil-M6 is also investigated by taking the whole suction side corrugated. The distance of corrugation from leading edge is 0.035c, 0.167c, 0.312c, 0.618c and 0.823c for airfoil M1, M2, M3, M4 and M5 respectively. Figs. 7(a) and 7(b) shows the mean skin friction coefficient for various airfoils at Re=1400 and 10000. The airfoil is represented in such a way that mid of the chord is designated at 0, while leading and trailing edge are designated at -0.5 and +0.5 respectively on the axis (for unit chord length).

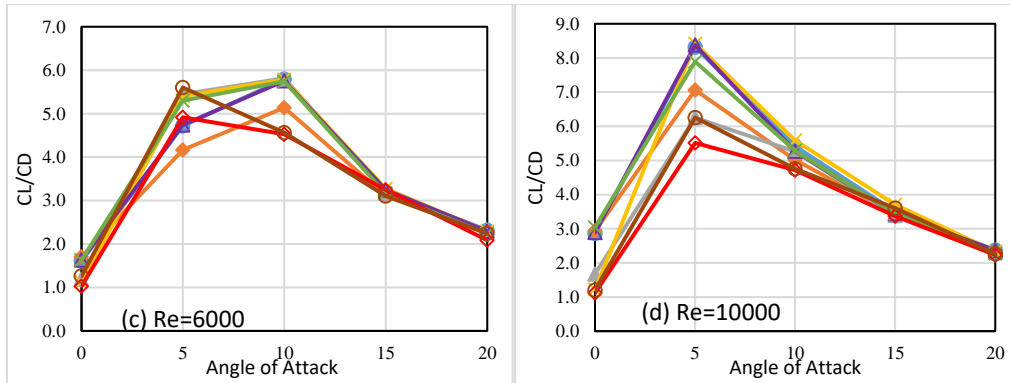**Figure 7(a):** Variation of time averaged mean skin friction coefficient at 0° angle of attack for various airfoils at Re=1400
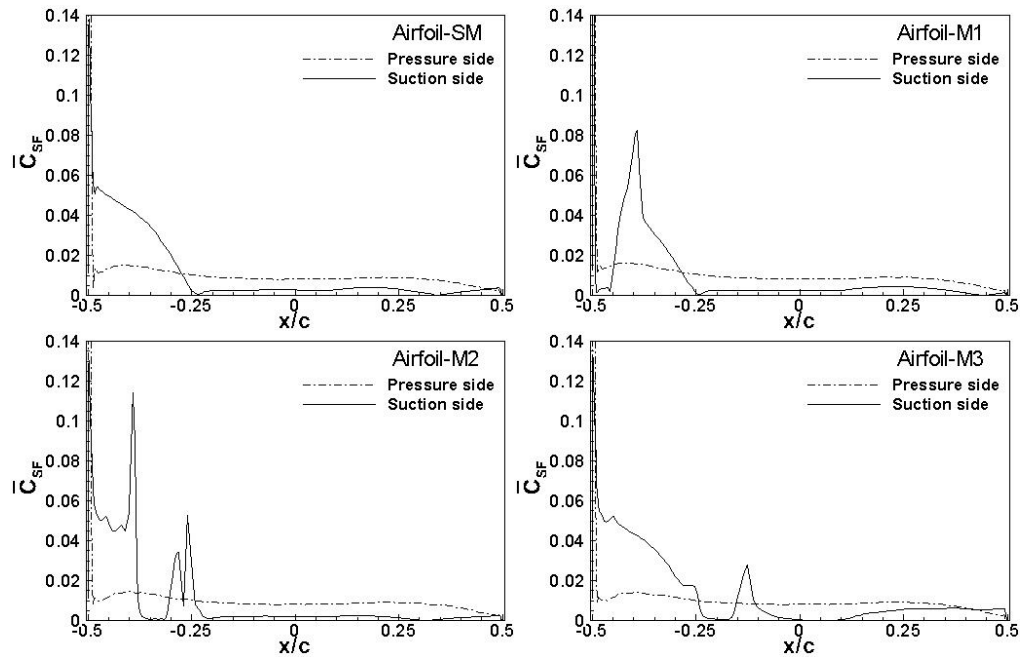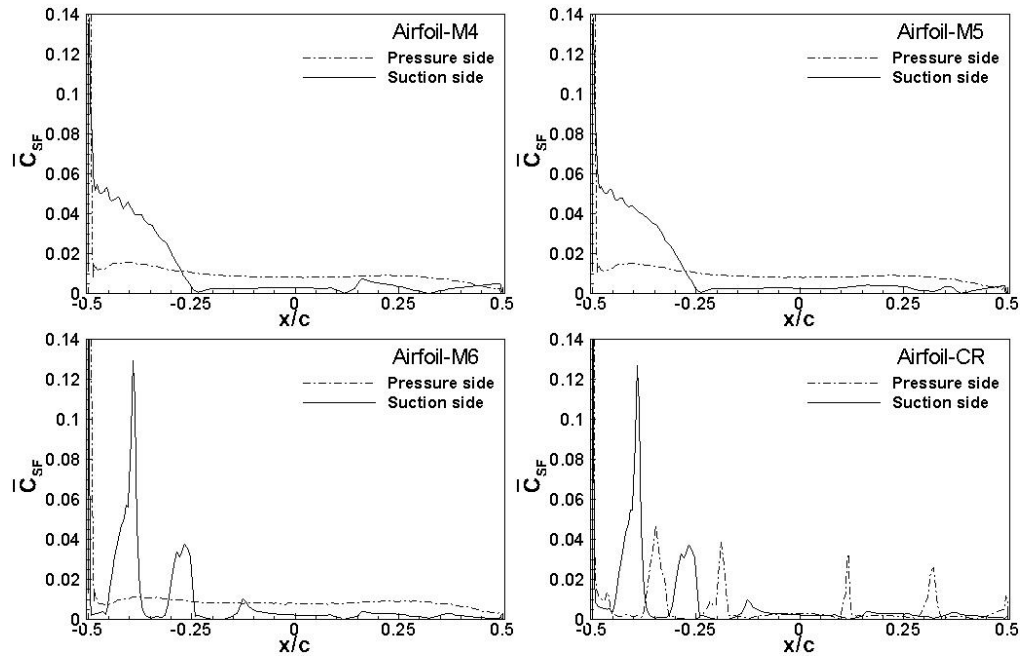
Figure 7(b): Variation of time averaged mean skin friction coefficient at 0° angle of attack for various airfoils at Re=10000

It is evident from the figure that the mean skin friction coefficient is considerably affected by the corrugation on the suction side of the airfoil. The shear drag distribution becomes more complex as the complexity of the airfoil geometry increases. There is peak of shear drag near the corrugation on the surface of the airfoil while for smooth airfoil there is no such peak and have smooth curve for mean skin friction drag. The most of the shear drag is found in the region of 0 to 0.25c from the leading edge of the airfoil. The shear is more on upper side (suction side) of the airfoil edge than on the lower side (pressure side) up to distance of 0.25c from leading edge and thereafter decreases and becomes nearly constant. Due to corrugation, there is a sudden rise and fall in shear drag distribution and for this reason in some cases the overall shear drag decreases. As shown in figure, the distribution of shear drag on the surface of airfoil is nearly similar at Re=1400 and Re=10000, but the magnitude is on higher side at Re=1400. It is also noticed that the Airfoil-M2 has the lowest shear drag among the airfoils having single corrugation.

At Re=10000 (Fig. 8), the streamlines pattern shows that vortex is trapped in corrugated valley and flow past the airfoil resembles the flow over the smooth airfoil. The flow separation occurs from downstream of the tip of one corrugation and gets reattached to upstream tip of next corresponding corrugation.

Figure 8: Time averaged mean streamline for Airfoil-CR at Re=10000 and 0° angle of attack

3.4 Gliding ratio

In a gliding flight, the $\bar{C}_L/\bar{C}_D$ is known as the gliding ratio which is an important aspect to measure the aerodynamic performance of forward flight. The ratio is plotted for all the eight airfoils at Re=150, 1400, 6000 and 10000 at various angle of attack as shown in Fig. 9. The best value of gliding ratio for CR is 1.87 at 15° angle of attack while the performance of all the other airfoils is nearly same with gliding ratio 1.73 at Re=150. At Re=1400 the highest performance is 3.82 for airfoil CR, 3.59 for M2 and lowest for M6 having gliding ratio 3.44. For other airfoils the value is nearly same of about 3.52 at 10° angle of attack. At Re= 6000, the gliding ratio is 5.60 and 4.92 for CR and M6 at 5° angle of attack, while other airfoils show higher performance at 10° with gliding ratio about 5.79 for SM, M2 and M3. M4 and M5 have gliding ratio of 5.75 and M1 have a value of 5.12. At 10°, M6 and CR have gliding ratio of 4.55. Comparing the airfoils at Re=10000 and 5° angle of attack, the highest performance is found for airfoils M3, M4 and SM having gliding ratio of over 8, while for CR gliding ratio is estimated as 6.25.

Figure 9: Variation of gliding ratio ($\bar{C}_L/\bar{C}_D$) with angle of attack for different airfoils at (a) Re=150 (b) Re=1400 (c) Re=6000 & (d) Re=10000

Fig. 9 shows that the gliding ratio is best for Airfoil-CR at low Reynolds number, with increase in angle of attack at Re=150, $\bar{C}_L/\bar{C}_D$ ratio increases and beyond 15° it falls due to an increase in the magnitude of drag coefficient. The main reason for rise in total drag is increase in pressure drag due to increase in frontal area against the inflow stream while the viscous drag is comparatively very small. At Re=1400 and 10000 the fall in gliding ratio is after 10°and 5° respectively. At Re=6000, for airfoils M6 and CR the gliding ratio falls after 5° while for other airfoils it falls after 10°.

3.5 Spatio-temporal dynamics

To realize the effect of MAVs of different sizes, moving at different velocities and viscosity of fluid, a numerical study at different Reynolds number is carried out. Fig. 10 shows the time-averaged streamline pattern for airfoil SM, M6 and CR at various Reynolds number. Plot shows that at Re=150, Airfoil-SM have no vortex formation on the surface of the airfoil while airfoil M6 and CR have trapped vortex of weak strength in corrugation near the leading edge and the flow is mostly attached to the surface. As the Reynolds number increases to 1400, the vortex is formed in all the corrugation and also on the surface of the airfoil and flow separation occurs. At Reynolds number higher than 1400, the vortex strength on the surface of the airfoil increases and separation region also increases. In addition, vortex shedding occurs at the trailing edge of the Airfoil-CR.

Re=1400

Re=150
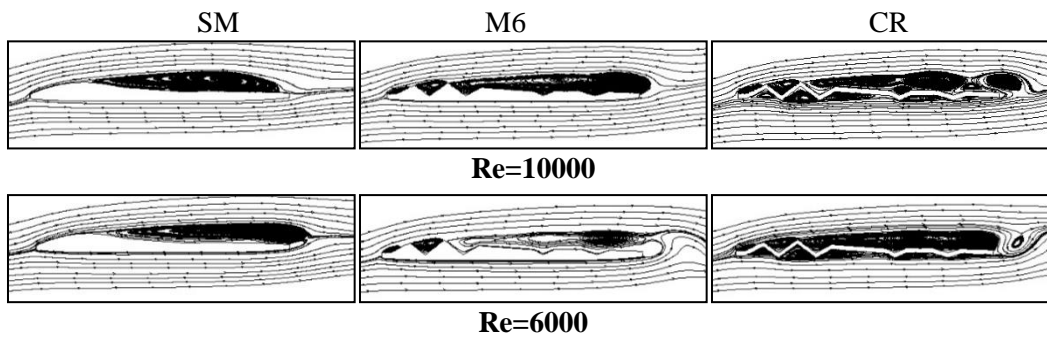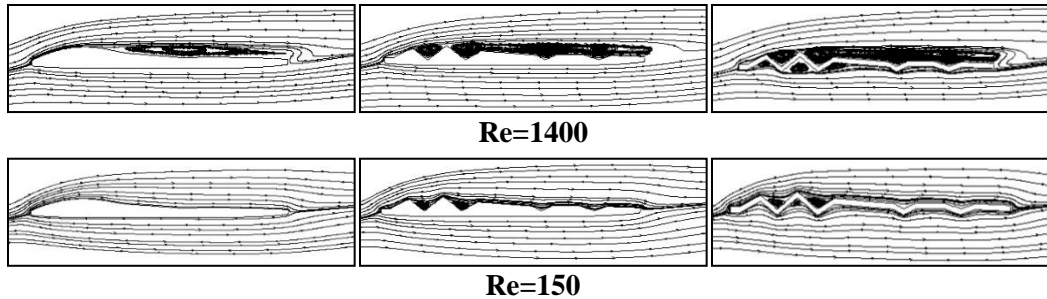
Figure 10: Time-average streamline plot of Airfoil-SM (left), Airfoil-M6 (middle) and Airfoil-CR (right) at 5° with Re=10000, 6000, 1400 and 150

A comparison of time-averaged lift and drag coefficients at 5° for different airfoils against the Reynolds number is shown in Fig. 11. The value of lift coefficient for airfoil SM and M4 are similar and follows a same trend at all Reynolds number. Up to Re=6000, the airfoil CR has the highest lift coefficient of about 0.44, while at Re=10000 the airfoil SM, M3, M4 and M5 have highest lift coefficient of about 0.59. The drag coefficient analysis shows that up to Re=1400, the drag coefficient are almost same and for higher Reynolds number there is small difference with airfoil M2 have lowest value in all airfoils.
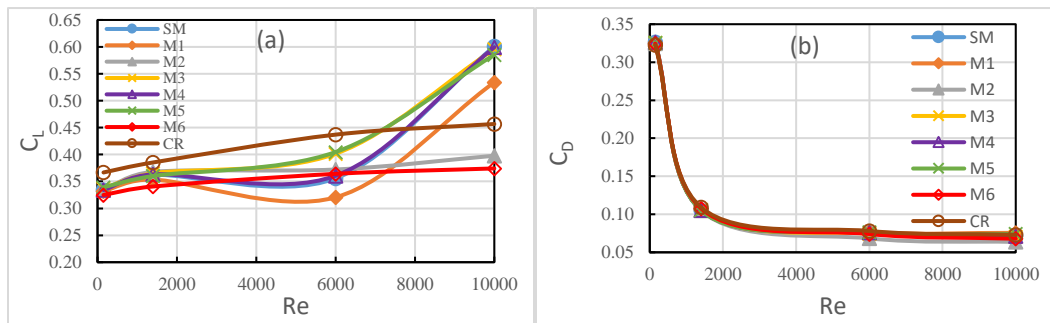
Figure 11: Time-Variation of time-averaged mean coefficient of (a) lift $\overline{C}_L$ and (b) drag $\overline{C}_D$ for various airfoils at 5^0 with Reynolds number

Fig. 12 shows the effect of Reynolds number on $\bar{C}_L/\bar{C}_D$ for various airfoils. The airfoil CR outperform other airfoils upto Re=6000 while the airfoil M1 performance is lowest. Similar to lift coefficient, the $\bar{C}_L/\bar{C}_D$ pattern also matches for airfoil SM and M4. At Re= 10000, the CR performance declines and airfoil SM, M3 and M4 have the highest performance. The airfoil M6 has lowest performance and airfoil M2 and CR have nearly same performance.
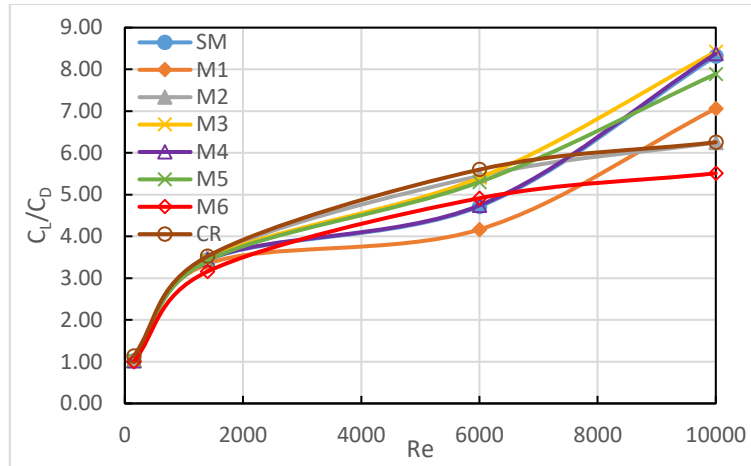
Figure 12: Time-average mean gliding ratio($\bar{C}_L/\bar{C}_D$) for various airfoils at 5° with Reynolds number

4 Conclusion

Numerical study of corrugation is carried out by taking fully corrugated Airfoil-CR, a smooth airfoil (SM) constructed by splines joining the corners of corrugation on Airfoil-CR, an airfoil having upper side corrugated and lower side smooth (M6), and five other airfoils having single corrugation on upper surface (M1 to M5) each corresponding to Airfoil-CR. The analysis of corrugation shows the shear drag decreases due to the corrugated valley but the pressure drag increases which increases the overall drag coefficient as compared to smooth airfoil due to flow trapped in the corrugated valley. Comparing the airfoils, CR and M6 have highest drag coefficient followed by M2 and M3 airfoil in order. The flow is steady at Re=150 for the considered range of angle of attack. At Re=10000, the flow is unsteady even at 0° angle of attack except for airfoil SM and M4 which have steady flow. This indicates that at high Reynolds number, due to the presence of corrugation (airfoil M1, M2, M3 and M5) flow becomes oscillatory and consequently results in unsteady flow. The airfoil CR has highest lift coefficient at Re=150 and 1400 while airfoil M6 have a lowest value at all Reynolds number, while other airfoils have nearly similar values. The corrugated airfoil performance declines at higher Re=10000, and smooth airfoil outperform the others.

References

Alexander, D. E. (1984): Unusual phase relationships between the forewing and hind wings in flying dragonflies. *Journal of Experimental Biology*, vol. 109, pp. 379-383.

Anwer, S. F.; Hasan, N.; Sanghi, S.; Mukherjee, S. (2009): Computation of unsteady flows with moving boundaries using body fitted curvilinear moving grids. *Computers and Structures*, vol. 87, no. 11-12, pp. 691-700.

Birch, J.; Dickinson, M. (2001): Spanwise flow and the attachment of the leading-edge vortex on insect wings. *Nature*, vol. 412, pp. 729-733.

Brodsky, A. K. (1994): *The Evolution of Insect Flight*. Oxford University Press, New York.

Chen, Y. H.; Skote, M. (2016): Gliding performance of 3-D corrugated dragonfly wing with spanwise variation. *Journal of Fluids and Structures*, vol. 62, pp. 1-13.

Ellington, C. (1984b): The aerodynamics of hovering insect flight: II. Morphological parameter. *Philosophical Transactions of the Royal Society*, vol. 305, pp. 17-40.

Ennos, A. R. (1995): Mechanical behaviour in torsion of insect wings, blades of grass and other cambered structures. *Proceedings of the Royal Society of London Series B: Biological Sciences*, vol. 259, pp. 15-18.

Hasan, N.; Anwer, S. F.; Sanghi, S. (2005): Computation of unsteady flows with moving boundaries using body fitted curvilinear moving grids. *Journal of Computational Physics*, vol. 206, no. 2, pp. 661-683.

Kesel, A. B.; Philippi, U.; Nachtigall, W. (1998): Biomechanical aspects of the insect wing: an analysis using the finite element method. *Computers in Biology and Medicine*, vol. 28, pp. 423-437.

Kesel, A. B. (2000): Aerodynamic characteristics of dragonfly wing sections compared with technical aerofoils. *Journal of Experimental Biology*, vol. 203, pp. 3125-3135.

Kim, W. K.; Ko, J. H.; Park, H. C.; Byun, D. (2009): Effect of corrugation of the dragon fly wing on gliding performance. *Journal of Theoretical Biology*, vol. 260, pp. 523-530.

Kunz, P. J.; Kroo, H. (2001): Analysis and design of airfoils for use at ultra-low Reynolds numbers. *Fixed and Flapping Wing Aerodynamics for Micro Air Vehicles Applications: Progress in Astronautics and Aeronautics*, vol. 195, pp. 35-60.

May, M. L. (1991): Dragonfly flight: Power requirements at high speed and acceleration. *Journal of Experimental Biology*, vol. 158, pp. 325-342.

Meng, X. G.; Sun, M. (2013): Aerodynamic effects of wing corrugation at gliding flight at low Reynolds numbers. *Physics of Fluids*, vol. 25, no. 7, pp. 1-15.

Mingallon, M.; Ramaswamy, S. (2011): The architecture of the dragonfly wing: A study of the structural and fluid dynamic capabilities of the ansoptera's forewing. *Proceedings of the ASME 2011 International Mechanical Engineering Congress & Exposition*, vol. 2, pp. 723-730.

Norberg, R. A. (1972): The pterostigma of insect wings an inertial regulator of wing pitch. *Journal of Comparative Physiology*, vol. 81, pp. 9-22.

Okamoto, M.; Yasuda, K.; Azuma, A. (1996): Aerodynamic characteristics of the wings and body of a dragonfly. *Journal of Experimental Biology*, vol. 199, pp. 281-294.

Ruppell, G. (1989): Kinematic analysis of symmetrical flight maneuvers of odonata. *Journal of Experimental Biology*, vol. 144, pp. 13-42.

Shyy, W.; Liu, H. (2007): Flapping wings and aerodynamic lift: The role of leading-edge vortices. *AIAA Journal*, vol. 45, no. 12, pp. 2817-2819.

Tuncer, I. H.; Kaya, M. (2003): Thrust generation caused by flapping airfoils in a biplane configuration. *Journal of Aircraft*, vol. 40, no. 3, pp. 509-515.

Vargas, A.; Mittal, R. (2004): A computational study of the aerodynamic performance of a dragonfly wing. *AIAA-2319, 2nd Flow Control Conference*, Portland, Oregon.

Vargas, A.; Mittal, R.; Dong, H. (2008): A computational study of the aerodynamic performance of a dragon fly wing section in gliding flight. *Bioinspiration & Biommetics*, vol. 3, no. 2, pp. 1-13.

Vogel, S. (1957): Flight in drosophila: III. Aerodynamic characteristics of fly wing and wing models. *Journal of Experimental Biology*, vol. 46, pp. 431-443.

Wootton, R. J. (1992): Functional morphology of insect wings. *Annual Review of Entomology*, vol. 37, pp. 113-140.

Wakeling, J.; Ellington, C. (1997a): Dragonfly flight: I. Gliding flight and steady-state aerodynamic forces. *Journal of Experimental Biology*, vol. 200, pp. 543-556.